The Color and Stellar Mass Dependence of Small-Scale Galaxy Clustering in SDSS-III BOSS

Jamie A. Law-Smith[1], Daniel J. Eisenstein[1]

ABSTRACT

We measure the correlation of clustering to color and stellar mass in spectroscopic galaxies at $0.6 < z < 0.65$ using data from the Baryon Oscillation Spectroscopic Survey (BOSS) component of the Sloan Digital Sky Survey (SDSS-III). The clustering strength of each spectroscopic galaxy is measured as the number of photometric galaxies found within a specified radius annulus around it. We cross-correlate 66,657 (after redshift selection) spectroscopic galaxies with 6,625,645 imaging galaxies to measure clustering coefficients w_{red} and w_{blue} for red and blue galaxies (defined as $g - i >$ or < 2.35). We find the ratio of these coefficients, w_{red}/w_{blue}, to be 1.921 ± 0.11 in our smallest annulus of 75-125 kpc. At our largest radii (2-4 Mpc), we find w_{red}/w_{blue} to be 1.243 ± 0.05. Red galaxies therefore have denser environments that their blue counterparts at $z \approx 0.625$, and this effect heightens with decreasing radius. Irrespective of color, we find that w does not obey a simple power law relation with radius, showing a dip around 1 Mpc attributable to the transition from one- to two-halo regimes in HOD models. Holding mass fixed, we find a clear differentiation between clustering in red and blue galaxies, showing that clustering is not solely determined by stellar mass. Holding color fixed, we find that clustering increases with mass, and that this relationship is especially strong in red galaxies at small scales (a factor of 2 effect).

1. Introduction

Galaxies have many observable properties, such as position, redshift, color, luminosity, and stellar mass. These properties are related to the environment hosting the galaxies—usually a dark matter halo. Halos are bound dark matter structures that form in gravitational collapse and act as sites for galaxies to form and evolve. Galaxies with different properties might map their underlying dark matter distribution differently. If richer galaxy clustering occurs in regions of denser dark matter, we can learn about the relationship between galaxy properties and large-scale structure by analyzing the relationship between galaxy properties and clustering.

Besides helping us better understand the relationship between galaxies and halos, these types of studies can also shed light on galaxy formation and evolution. Clustering has been studied at

[1]Center for Astrophysics, Harvard University, 60 Garden St., Cambridge, MA 02138

low redshifts ($z < 0.25$) with the original Sloan Digital Sky Survey (Zehavi et al. 2011). In looking at intermediate redshifts ($0.6 < z < 0.65$), we can learn if and how the relationship between clustering and properties evolves over time. This study will also help to confirm or refute—via a different method (cross-correlation rather than auto-correlation)—studies made recently using the same datasets and redshift range (Guo et al. 2013).

In this paper we examine how galaxies' clustering (i.e., the density of neighboring galaxies) scales with their color and mass. We do this by cross-correlating spectroscopic and photometric datasets from the BOSS component of SDSS-III.

SDSS is a large-scale imaging and spectroscopic redshift survey, using a 2.5m wide-angle optical telescope at Apache Point Observatory in New Mexico, US. SDSS uses five filters (u, g, r, i, and z, with magnitude limits of 22.0, 22.2, 22.2, 21.3, and 20.5 respectively)—we use the g and i filters to assign galaxy color. We are using data from the BOSS component of SDSS-III. BOSS covers over 10,000 square degrees of sky, obtaining the redshifts of 1.5 million luminous galaxies with $z < 0.8$.

Clustering dependence on galaxy properties was understood early on as a density-morphology relation, where an increasing elliptical and S0 population and a corresponding decrease in spirals was associated with increasing cluster density (Dressler 1980). SDSS offers the largest statistical sample to date, enabling us to investigate more specific questions, such as the relationship between clustering and color or luminosity. With an early SDSS spectroscopic sample, clustering was found to depend on luminosity for red galaxies but not for blue galaxies (Hogg et al. 2002). In addition, red galaxies were found to inhabit highly over-dense regions. For luminous red galaxies, a very strong luminosity-clustering dependence was found: up to a factor of 4 in clustering amplitude over a factor of 4 in luminosity (Eisenstein et al. 2005). With the completion of the original SDSS survey, we obtained more definitive results on the clustering dependence on color and luminosity for $z < 0.25$. Clustering was found to increase slowly with luminosity for $L < L_*$ and more rapidly for higher luminosities; clustering was also found to have a continuously increasing trend with color from blue to red (Zehavi et al. 2011).

With the SDSS-III BOSS data, the same clustering studies were made in the redshift range $0.43 < z < 0.7$ (Guo et al. 2013). Clustering was found to depend clearly on luminosity and color, with more luminous and redder galaxies generally exhibiting stronger clustering. This clustering dependence on luminosity and color has been interpreted using halo occupation distribution (HOD) models (Zehavi et al. 2005). The HOD model fits the correlation results better than a power law, and explains inflections at larger radii as a transition from one- to two-halo regimes. The HOD model explains the color dependencies of clustering: less massive halos have blue central galaxies, while more massive halos have red central and satellite galaxies. The fraction of blue central galaxies decreases with increasing luminosity and host halo mass.

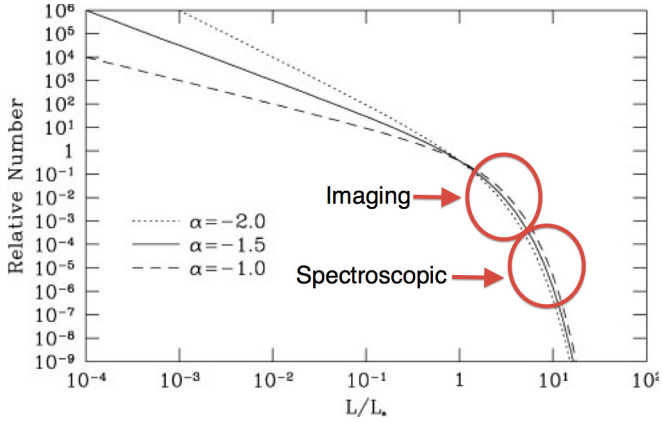

Fig. 1.— Rough sketch of regions of Schecter luminosity curve occupied by spectroscopic and imaging datasets. Original image from Schneider (1996).

2. Methods

2.1. Data

We use spectroscopic and imaging datasets from the BOSS component of SDSS-III. The spectroscopic dataset is from the DR10 (Data Release 10) footprint and the imaging is from DR9. Our stellar masses are derived in Chen et al. (2012). These are the Wisconsin stellar masses, using templates from Bruzual & Charlot (2003). BOSS spectra are fit to a set of principal components derived from a large set of model spectra. From the mass to luminosity ratio of the best-fit model, SDSS i-band cmodel magnitude is converted to stellar mass. The spectroscopic dataset has high luminosity ($i < 19.9$) and low number density ($\bar{n} = 1.2 \times 10^{-4} h^3$ Mpc^{-3} comoving, at our redshift) (Anderson et al. 2012), while the photometric dataset has lower luminosity ($19.9 < i < 20.9$) and higher number density ($\bar{n} = 10^{-3} h^3$ Mpc^{-3}). Figure 1 shows a cartoon illustrating (very roughly) the different regions of the Schecter luminosity curve occupied by these two datasets.

Both datasets are complete enough for our purposes: they contain many objects and span a large portion of the sky. Figure 2 shows plots of RA vs. Dec for both datasets. The survey does not image sky containing galactic dust, the galactic plane (roughly $|b| < 25°$), or sky in southern declinations. Zooming in on a smaller patch of sky, as shown in Fig. 3, we see that several smaller patches are also masked—this could be due to bright foreground stars/galaxies or poor imaging (bad seeing, bad sky brightness, jumps in the telescope tracking, etc.). We use a map of the masked regions of the imaging dataset (defined in Ross et al. 2011) in order to account for this (the strategy is described in the subsequent section).

From the full imaging and spectroscopic datasets, we cut away regions of higher dust extinction and some smaller regions of poor data quality (spectroscopic target selection defined in Dawson et al. 2013). We also perform color and flux cuts that select for higher redshift galaxies. The main

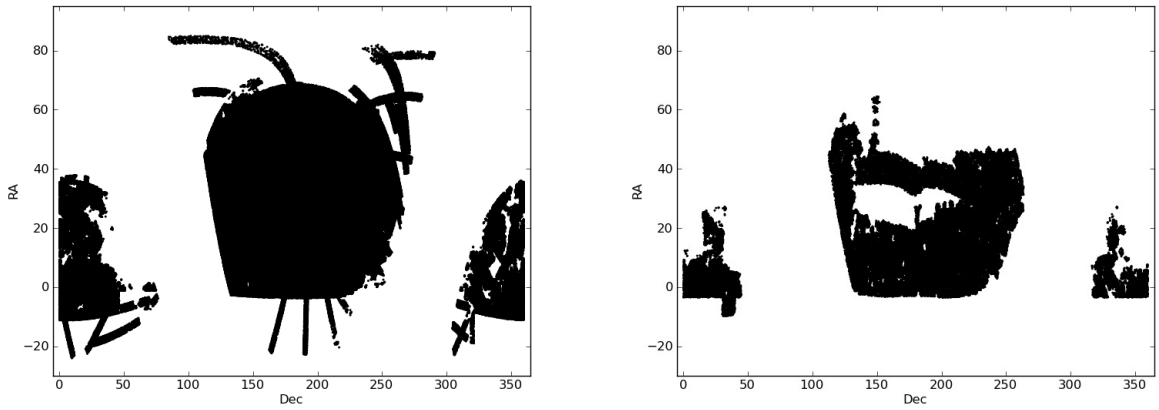

Fig. 2.— RA vs. Dec for imaging (left) and spectroscopic (right) datasets.

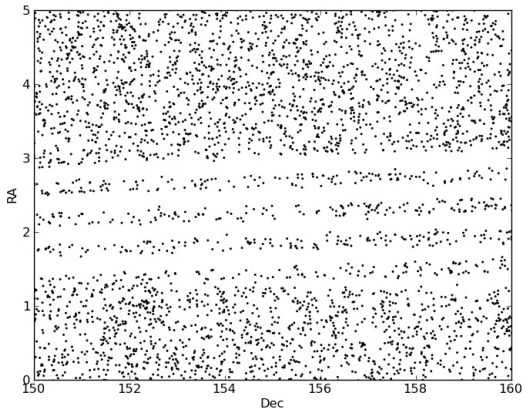

Fig. 3.— RA vs. Dec for imaging dataset, zoomed in on a smaller patch of sky, showing masked regions.

color cut is on the quantity $d_\perp = (r - i) - (g - r)/8$ (Dawson et al. 2013). In the spectroscopic dataset, we require $d_\perp > 0.55$; for the imaging we require $d_\perp > 0.6$. This cut highly favors $z > 0.45$ galaxies. This is because galaxies lose flux in the g band (and so $g - i = -2.5 \log(f_i/f_g)$ becomes larger) as they increase in redshift, and this behavior is sharpest as the 4000Å break passes through the g band. The tighter requirement on $d_\perp$ for imaging galaxies is because the scatter in observed colors is larger for faint objects, making it more likely that low redshift objects scatter into the cut. For the spectroscopic data, we only use the CMASS sample (as opposed to LOWZ). All told, this gives us about 6.6 million imaging galaxies and 517 thousand spectroscopic galaxies, over areas of 9432 and 6612 square degrees respectively.

We choose $g - i = 2.35$ as the cutoff between blue and red spectroscopic galaxies (blue being

	Imaging	Spectroscopic
apparent magnitude	$19.9 - 20.9$	< 19.9
number density [h^3 Mpc^{-3}]	10^{-3}	1.2×10^{-4}
number of galaxies	6,625,645	517,425
area [deg^2]	9432	6612

Table 1: Properties of imaging and spectroscopic datasets. Note that only 66,657 spectroscopic galaxies pass our redshift selection.

$g - i < 2.35$, red being $g - i > 2.35$). Observing the behavior of spectroscopic galaxies on a $r - i$ vs. $g - r$ plot with increasing redshift, we see that this is a reasonable choice. This progression is shown in Fig. 4, with the $g - i = 2.35$ line in green and the $d_\perp > 0.55$ cut in red. After $z = 0.45$, galaxies tend to move parallel to the $g - i$ line with increasing redshift—this is good, as our red and blue populations do not drift into one another. At lower redshifts, the sample (particularly in the blue) is partially cut off, but at $0.6 < z < 0.65$ (the redshift range we select), there is a good population of red and blue galaxies. In calculating color-band fluxes, we correct for reddening due to dust.

The mass distribution of the spectroscopic dataset is shown in Figure 5, where it is plotted against color in $g - i$. Mass is measured as the logarithm of the galaxy stellar mass in solar units. Our blue galaxies are on average less massive than our red galaxies. We choose to isolate mass in bins of 0.25, which gives us three reliable mass bins in blue (from 11-11.75) and four in red (from 11.25-12.25). Two of these are overlapping, allowing us to compare clustering vs. color in fixed mass bins.

Table 1 summarizes the basic properties of the two datasets we use in this paper. After applying our redshift selection of $0.6 < z < 0.65$, we are left with 66,657 spectroscopic galaxies, 14,480 of which are blue and 52,172 of which are red.

We could conduct an auto-correlation analysis using only the spectroscopic dataset. Instead we study the cross-correlation between this and the imaging dataset. By including the fainter imaging sample, we increase the number density of environment galaxies by a nearly a factor of ten. Conducting a cross-correlation analysis allows us to measure clustering in smaller radius annuli and keep our errors low.

In this paper we examine the color- and stellar mass-clustering relationship for spectroscopic galaxies at $0.6 < z < 0.65$. It is easy to make this selection on the spectroscopic galaxies—we know their redshifts. This is not the case for the imaging galaxies, though. Fortunately, we are only concerned with the excess correlation of imaging galaxies, which is unaffected by foreground or background galaxies. Any fluctuations in these foreground/background imaging galaxies are not correlated with signals we are looking for in our redshift range.

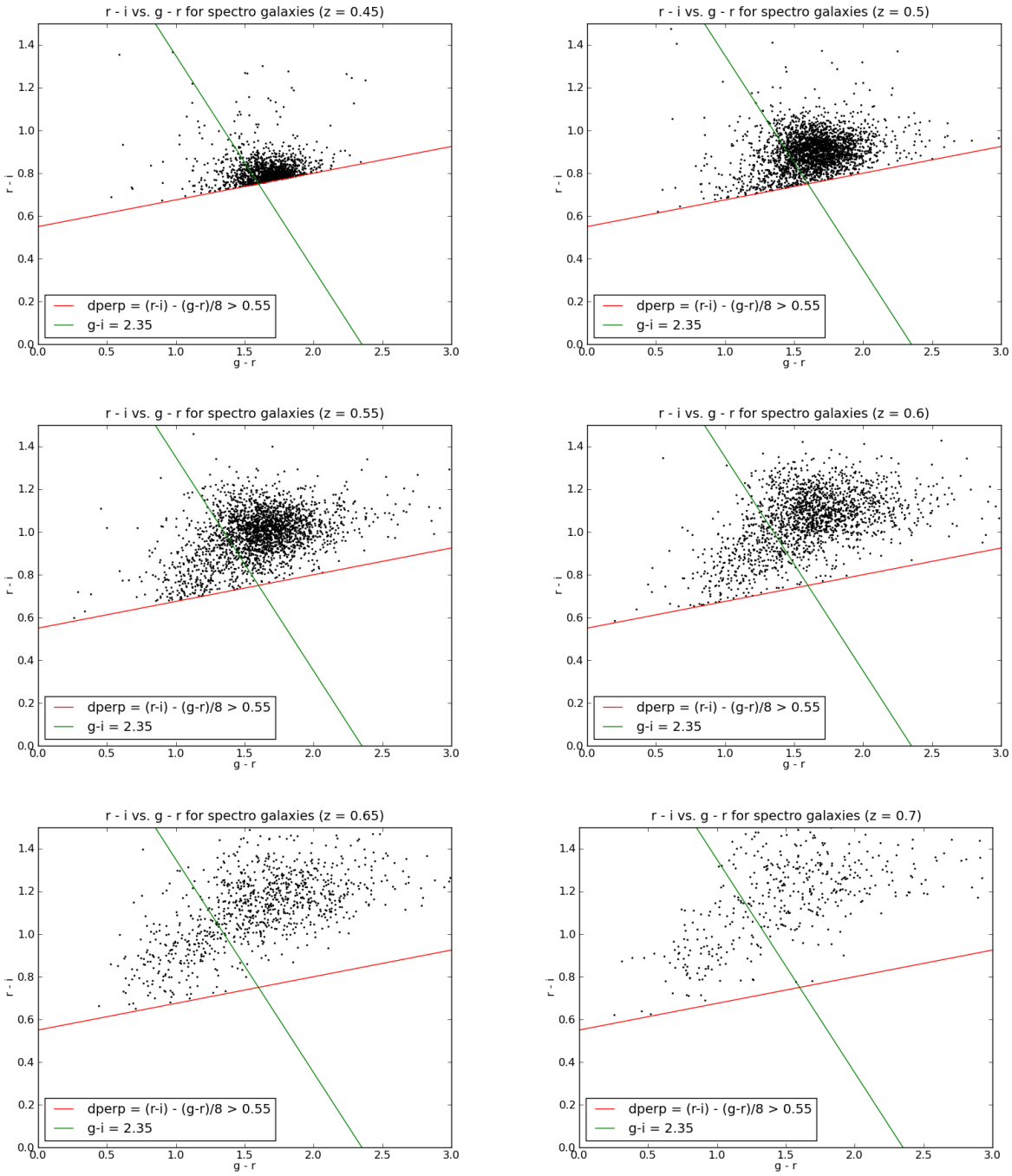

Fig. 4.— Redshift progression of spectroscopic galaxies on $r-i$ vs. $g-r$ plot. The $d_\perp$ cut is shown in red and the divide between blue and red galaxies in green. At $0.6 < z < 0.65$, we have good populations of red and blue galaxies, with neither being cut off.

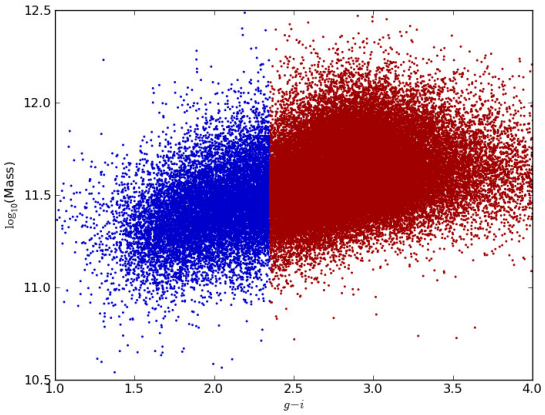

Fig. 5.— Mass distribution vs. color $(g-i)$ for spectroscopic dataset at $0.6 < z < 0.65$. Blue galaxies are on the left half of the plot and red on the right.

In practice, the background of imaging galaxies is not very significant, simply because their faintness prevents high-z galaxies from showing up on the survey. The imaging dataset will contain very few galaxies at $z > 0.9$. $z < 0.45$ galaxies, on the other hand, are eliminated by the $d_\perp$ cut. It is useful to reduce the number of high and low redshift imaging galaxies because while they do not contribute to our correlation signal, they do contribute to the noise (by increasing the number of objects in our radius bins, we increase the variance in the counts).

While we expect the redshift distribution of the imaging dataset to be similar to that of the spectroscopic (shown in Fig. 6), we do not know it. If we knew the average 3-D density of the imaging galaxies at our redshift, we could make some additional interesting measurements. Again, though, we do not need to know the imaging galaxies' redshift distribution for our calculation. We are concerned with differential comparisons between spectroscopic galaxies, making only the ratio of their environments important. Any uncorrelated addition to the density of imaging galaxies around each spectroscopic galaxy will not impact excess correlation—the parameter we are after.

2.2. Strategy

Our goal is to determine how the clustering of the spectroscopic galaxies changes with their color and stellar mass. First, we define color according to the difference in magnitude in the g and i bands: we denote $g - i < 2.35$ as blue and $g - i > 2.35$ as red. We then count the number of imaging galaxies around each spectroscopic galaxy, comparing between the blue and red selections. We do this for different angular bins in order assess how the clustering dependence on color changes with radius. The annuli, in terms of proper radii from each spectroscopic galaxy, are: 125-250 kpc, 250-500 kpc, 500-1000 kpc, 1-2 Mpc, and 2-4 Mpc. Note that the diameter of a galaxy cluster is

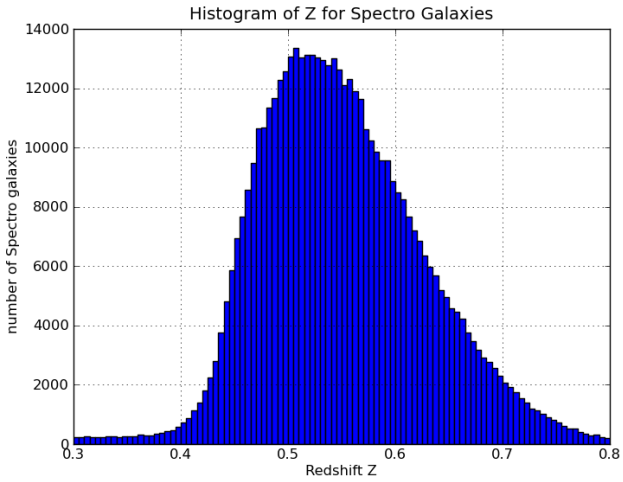

Fig. 6.— Redshift distribution of spectroscopic dataset.

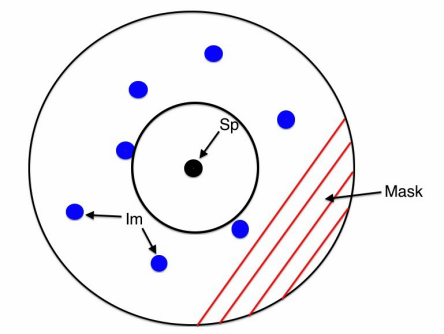

Fig. 7.— Cartoon of counting setup. The inner and outer rings represent the bounds of a particular radius annulus.

1-2Mpc. Knowing that clusters are predominantly composed of red galaxies, we might expect red galaxies to have denser environments than blue galaxies. We perform this same analysis in different mass bins, keeping color fixed. We also compare clustering vs. color in fixed mass bins.

Our first problem is that the survey is imperfect—many regions are masked (due to foreground stars or poor imaging). Using our map of the imaging mask, we can generate random points across all masked regions, and count the number of points that appear in any radial bin. This gives us an estimate of the fraction of a bin that is masked. The density of the mask points is high, with 17,767,741 points over 6108 deg^2 of sky in the mask map. For each spectroscopic galaxy, the picture looks something like Fig. 7, where we count the number of imaging galaxies within a specified radius annulus of the galaxy, accounting for the masked regions (enlarged here for clarity).

Accounting for the mask, the average number of imaging galaxies around each spectroscopic

galaxy should scale as $N_{Sp,j} \propto (1+w)A = (1+w)(A_{total} - A_{mask})$, where A_{total} is the total area between the inner and outer radii from the spectroscopic galaxy and A_{mask} is the masked area in this region. If this number of counts is uncorrelated with whatever selection j we make on the spectroscopic galaxies, we expect the correlation coefficient w to be zero. The stronger the correlation of the clustering with our selection j, the larger w is. In this paper, we ask how w changes with color and stellar mass of the spectroscopic galaxies at different radii. We discuss the calculation of w more quantitatively below.

Let's define the average areal density of the imaging dataset to be $\bar{n}_I = N_I/A_I$, and the average areal density of the mask to be $\bar{n}_M = N_M/A_M$. For our datasets, $\bar{n}_I = 702/\mathrm{deg}^2$ and $\bar{n}_M = 2909/\mathrm{deg}^2$. Now for a spectroscopic galaxy in our selection j, for a specific angular bin $\theta_{out} - \theta_{in}$, we expect the following count of imaging galaxies:

$$\mathrm{Counts}_{j,\theta_{out}-\theta_{in}} = (1+w)n_I A_{cutout} = (1+w)n_I(\pi(\theta_{out}^2 - \theta_{in}^2) - \mathrm{Counts}_M/n_M)$$

Averaging over the set of j spectroscopic galaxies, we have

$$\langle \mathrm{Counts}_{j,\theta_{out}-\theta_{in}} \rangle = (1+w)\bar{n}_I(\pi(\theta_{out}^2 - \theta_{in}^2) - \langle \mathrm{Counts}_M \rangle/\bar{n}_M),$$

where $\langle x_i \rangle = \frac{1}{N}\sum x_i$ as usual. From this we can easily solve for w.

In calculating errors on our calculation of w, we estimate that the noise in our data is primarily due to poisson variance (or shot noise), rather than sample variance. Shot noise is proportional to $\sqrt{N_{gal}}$, giving a signal to noise ratio proportional to $N_{gal}/\sqrt{N_{gal}} = \sqrt{N_{gal}}$. At smaller radii, there are fewer imaging galaxies around each spectroscopic galaxy. $N_{gal} \propto R^2$, so the signal to noise scales with R. This dominates the sample noise contribution at low radii. The average counts of imaging galaxies around each spectroscopic galaxy are small (see Table 2), which is further motivation for relying only on shot noise.

Sample variance derives from the fact that not all regions of the sky are identical. One patch (sample) of the sky will vary slightly from the next. This effect also increases with increasing R, but more quickly than shot noise. So sample variance could dominate at larger R. While we ignored sample variance in this paper, we could calculate it by binning the sky into non-overlapping areas and computing the variance in w between these areas.

3. Results

Table 2 shows the average number of imaging counts around each spectroscopic galaxy for different bins in radius, for blue and red galaxies. It also lists the corresponding angles and areas, including masked area and number of masked points to see the scale of the masking (consistently

	R_{inner} [kpc]	R_{outer}	θ_{inner} [deg]	θ_{outer}	A [deg^2]	A_{masked}	A_{final}	N_{Im}	N_{Mask}
blue	62.5	125	0.0026	0.0051	0.000061	0.000000	0.000061	0.0901	0.0011
red								0.1336	0.0010
blue	125	250	0.0051	0.0102	0.000246	0.000003	0.000243	0.2588	0.0088
red								0.3552	0.0100
blue	250	500	0.0102	0.0204	0.000982	0.000024	0.000958	0.8724	0.0712
red								1.0116	0.0731
blue	500	1000	0.0204	0.0408	0.003930	0.000189	0.003740	3.0337	0.5508
red								3.2370	0.5368
blue	1000	2000	0.0408	0.0817	0.015718	0.001210	0.014509	11.1782	3.5186
red								11.4729	3.4884
blue	2000	4000	0.0817	0.1634	0.062873	0.005610	0.057263	42.7331	16.3196
red								43.3248	16.3873

Table 2: Imaging counts for red and blue galaxies in different annuli of radius.

R_{av} [kpc]	$w_{blue} \pm \sigma_{w,blue}$	$w_{red} \pm \sigma_{w,red}$	w_{red}/w_{blue}
93.75	1.1009 ± 0.0602	2.1152 ± 0.0382	1.9214 ± 0.1107
187.5	0.5190 ± 0.0263	1.0878 ± 0.0164	2.0957 ± 0.1108
375	0.2964 ± 0.0127	0.5043 ± 0.0074	1.7014 ± 0.0771
750	0.1546 ± 0.0066	0.2304 ± 0.0036	1.4902 ± 0.0678
1500	0.0967 ± 0.0037	0.1248 ± 0.0020	1.2905 ± 0.0535
3000	0.0623 ± 0.0023	0.0774 ± 0.0012	1.2431 ± 0.0498

Table 3: Correlation coefficient w, with errors, for red and blue galaxies in different angular annuli. The ratio w_{red}/w_{blue} increases with decreasing R.

less than 10% of a bin's area). We convert angles on the sky to transverse distances for each annulus, using $z = 0.625$ (the average redshift of our selection). The radii quoted are proper [distances].

There are on average more imaging neighbors to red spectroscopic galaxies than their blue counterparts. Table 3 presents this information in terms of the correlation coefficient w, along with the errors associated with its calculation (which are quite small).

R_{av} denotes the average radius of a particular annulus. Note that the annuli are nonintersecting. We expect w to be greater for red galaxies than blue ones, as galaxy clusters are made predominantly of red galaxies. w is much larger at smaller radii, indicating that the correlation between color and clustering is stronger at smaller scales. It is also useful to observe the ratio of w_{red} to w_{blue} (this is more interesting than simply the difference in magnitude between the two). This ratio is highest at small R, and it decreases with increasing R, as expected. w also approaches zero at larger R, which is also expected. As we increase the scale to greater than that of a galaxy cluster, the clustering dependence on color should weaken.

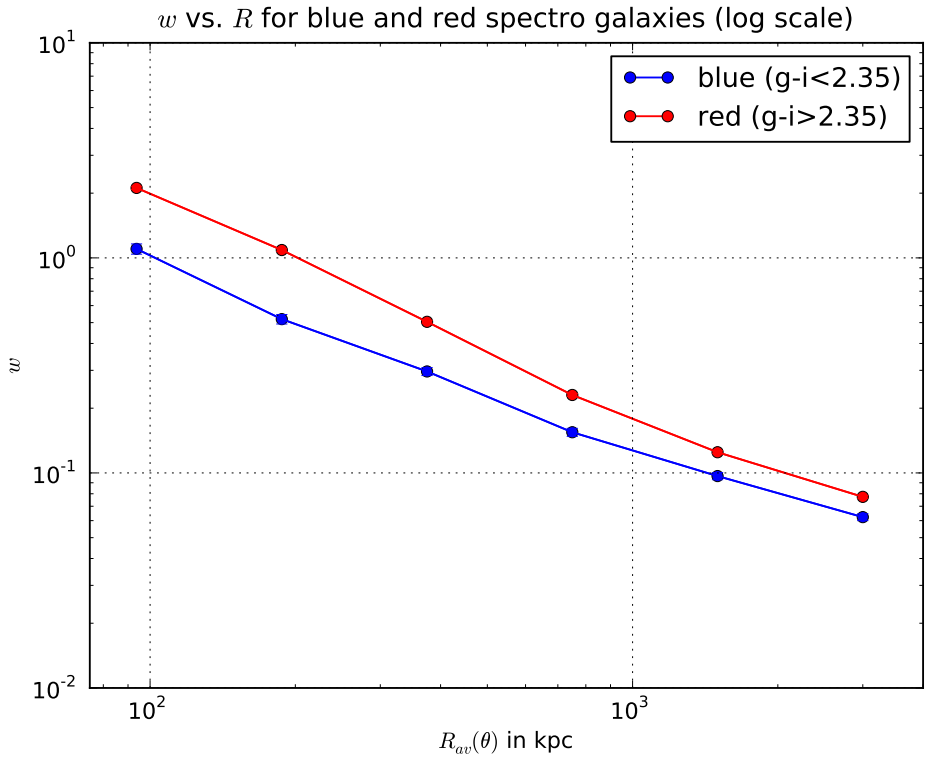

Fig. 8.— w for red and blue galaxies in different angular bins. The x axis plots R_{ave}, the average radius in each radius bin. The bins are nonintersecting.

The same information is presented graphically in Figure 8. The log scale highlights that $w_{red}/w_{blue} \to 1$ as R increases.

Figure 9, which plots Rw vs. R, lets us examine the relationship between w and R from another angle. Note that the error bars have been scaled up accordingly here. This plot shows that w and R do not have a simple power law relationship—if this was the case, the curve would be monotonic, as is indicated by the dashed lines. Around $R = 1$ Mpc, there is a pronounced dip in the curve, especially for red galaxies. This is interpreted in the HOD formalism as a transition to a two-halo regime. It makes sense that this should happen around 1 Mpc, the scale of a galaxy cluster.

We next investigate how galaxy clustering depends upon stellar mass. We do this by measuring the clustering coefficient in different mass bins for fixed color. Figure 10 shows this relationship for blue galaxies and Figure 11 shows it for red galaxies. Remember that mass is measured as the logarithm of the galaxy's stellar mass in solar units. In blue galaxies, we find a positive clustering-mass relationship between the first two mass bins, but not much differentiation between the top two mass bins. In red galaxies, the clustering-mass relationship is very strong, especially at small

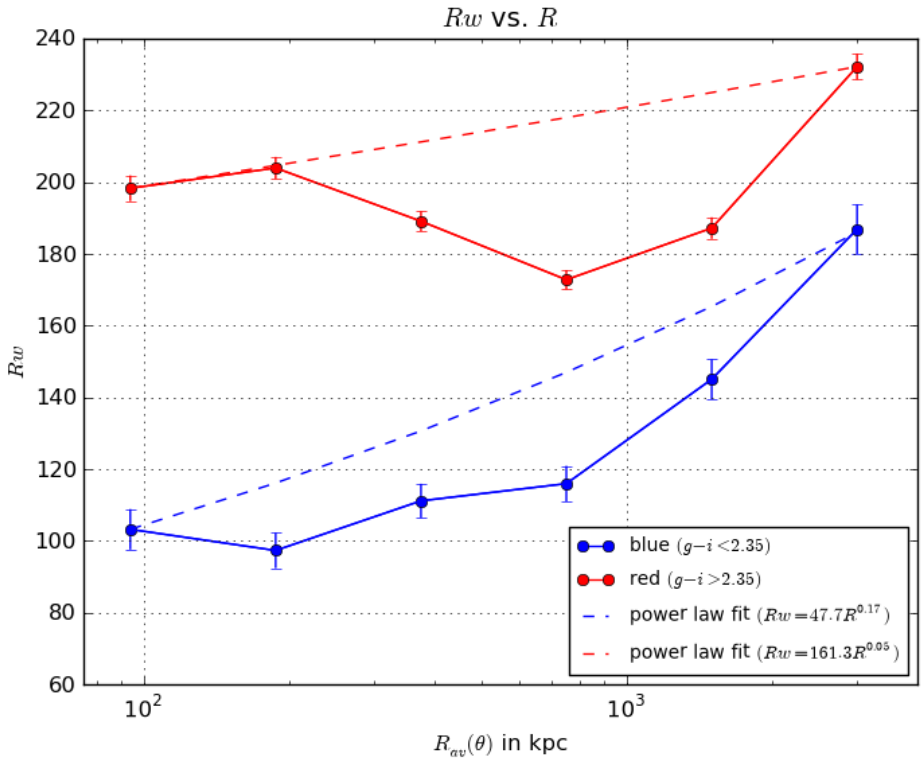

Fig. 9.— Rw vs. R. This shows that R and w do not obey a simple power law relation, with a pronounced dip around 1 Mpc.

scales, where there is over a twofold increase in clustering from the lowest to highest mass bin.

Another interesting question is whether the color-clustering relationship we found above holds for fixed mass. Figures 12 and 13 show Rw vs. R plots for galaxies with masses of 11.25-11.50 and 11.50-11.75 respectively. There is a clear difference in clustering between red and blue galaxies in the same mass bin, especially at smaller scales. This shows that clustering is not solely dependent on stellar mass.

4. Conclusions

We find that red galaxies at $0.6 < z < 0.65$ have denser environments than their blue counterparts, and that this behavior heightens at smaller radii. In the 125-250 kpc annulus, we find the ratio of the correlation coefficients w_{red}/w_{blue} to be 1.9214 ± 0.1107. This ratio decreases with increasing radius, with $w_{red}/w_{blue} = 1.2431 \pm 0.0498$ in the 2-4 Mpc annulus. That red galaxies have denser environments at $z \approx 0.625$ implies that massive halos (which exhibit denser clustering) have red central galaxies. The opposite appears to be true for blue galaxies: they are predomi-

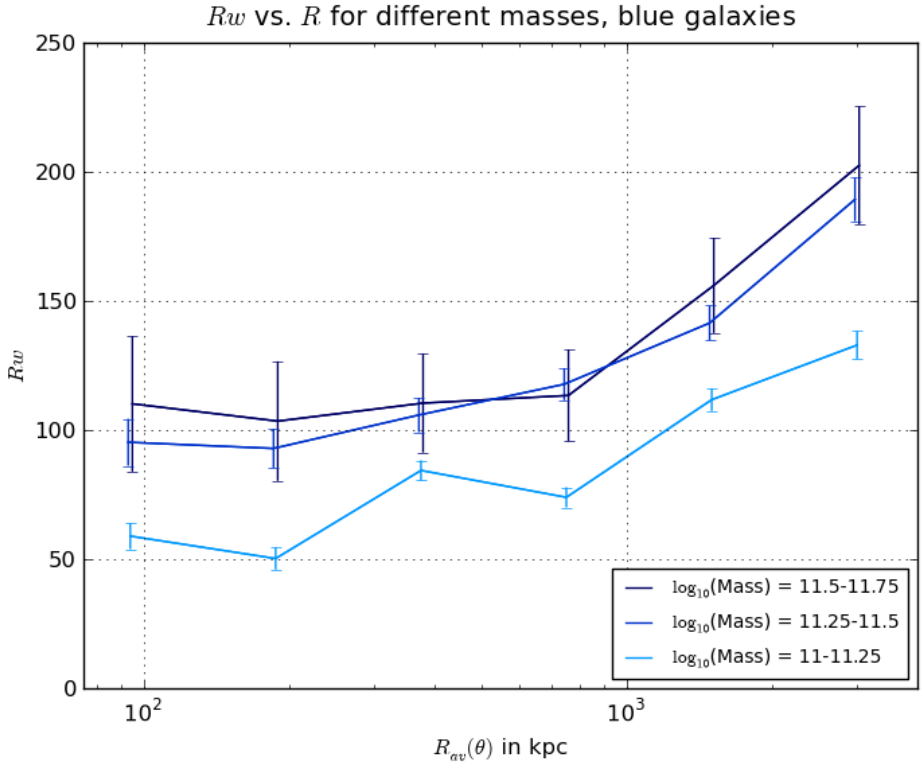

Fig. 10.— Rw vs. R for blue galaxies in different mass bins. Clustering increases with increasing mass, but there is not much difference between the highest two mass bins.

nantly found in lower mass halos, which promote lower clustering density. This has implications for theories of halo formation and evolution and their relationships to galaxy properties.

We were able to obtain very strong detections of the clustering in each subpopulation—the error bars on Figure 9 are impressively small. This plot clearly shows that the clustering deviates from a power law relation for both red and blue galaxies. The dip around 1 Mpc could be due to the change in environment from one- to two-halo systems.

Isolating mass into smaller bins, we find a clear differentiation between clustering in red and blue galaxies (especially at smaller scales), showing that mass is not the sole determinant of clustering. This rejects a simple model that halo mass begets stellar mass, independent of color. Holding color fixed, we find that clustering increases with mass, especially for red galaxies at small radii (where it is more than a factor of 2 effect).

For further study, we could conduct a similar analysis of the clustering dependence on galaxy luminosity. By isolating the spectroscopic sample into several luminosity bins, we could explore how galaxy clustering depends on this property. We expect stronger clustering around more luminous galaxies.

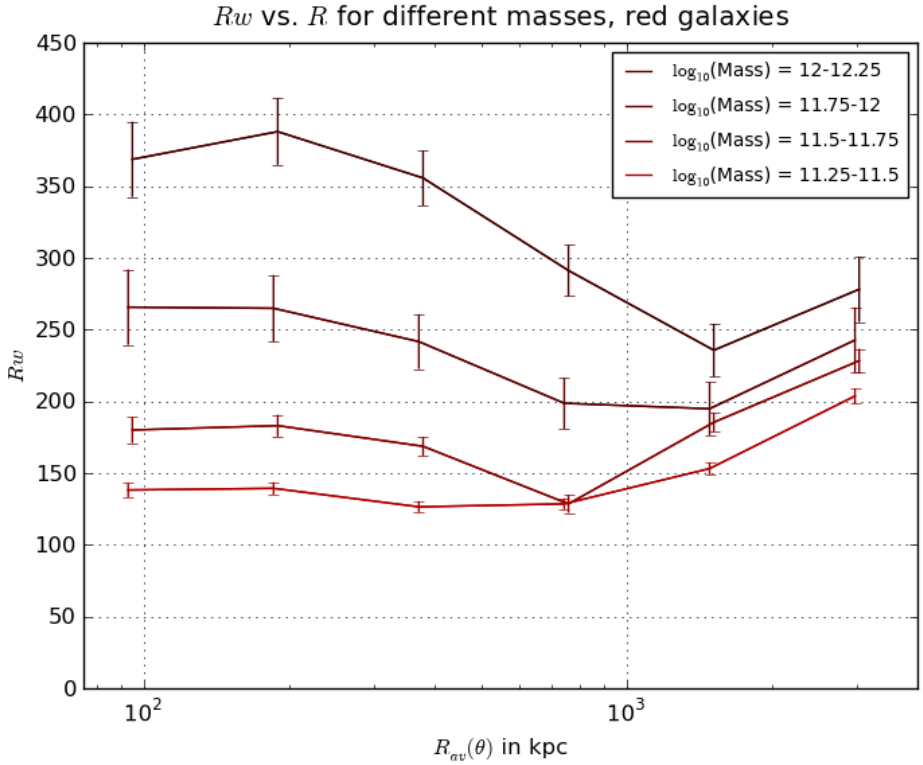

Fig. 11.— Rw vs. R for red galaxies in different mass bins. Clustering increases over twofold from lowest to highest mass at small scales.

We would like to thank Aaron Bray for extracting the imaging catalog from the Catalog Archive Server, applying the imaging mask to it, and generating the random points in the inverse mask. We would also like to thank Ashley Ross for providing the imaging mask, and the SDSS-III BOSS Galaxy Clustering Working Group for providing the catalog of spectroscopic galaxies.

REFERENCES

Anderson, L. et al. 2012, arXiv:1203.6594 [astro-ph.CO]

Bruzal, G. and Charlot, S. 2003, MNRAS, 344, 1000

Chen, Y.-M. et al. 2012, MNRAS, 421, 314

Dawson, K. S. et al. 2013, AJ, 145, 10

Dressler, A., 1980, ApJ, 236, 351

Eisenstein, D. J. et al. 2005, ApJ, 619, 178

Guo. H et al. 2013, ApJ, 767, 122

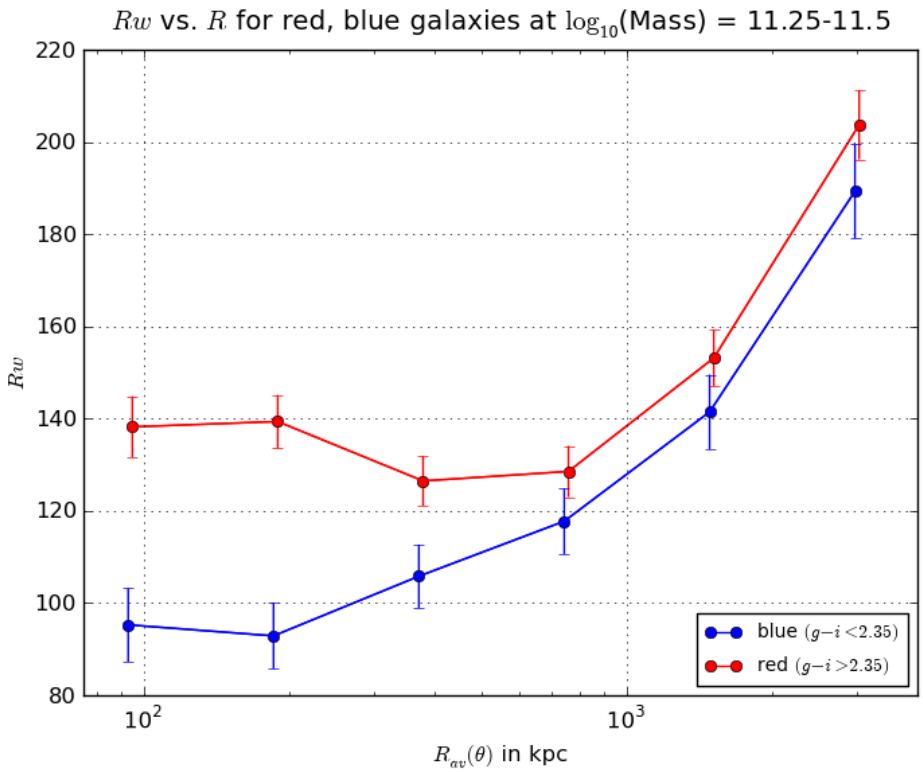

Fig. 12.— Rw vs. R for galaxies with $\log_{10}$(Mass) between 11.25 and 11.50. Mass is quoted in solar units. We see differentiation between clustering in red and blue galaxies, especially at smaller scales.

Hogg, D. W. et al. 2002, ApJL, 585, L5

Ross, A. J. et al. 2011, MNRAS, 417, 1350

Schneider, S. E. 1996, "HI Selection Effects and the Galaxy Mass Function"

Zehavi, I. et al. 2005, ApJ, 630, 1

Zehavi, I. et al. 2011, ApJ, 736, 59

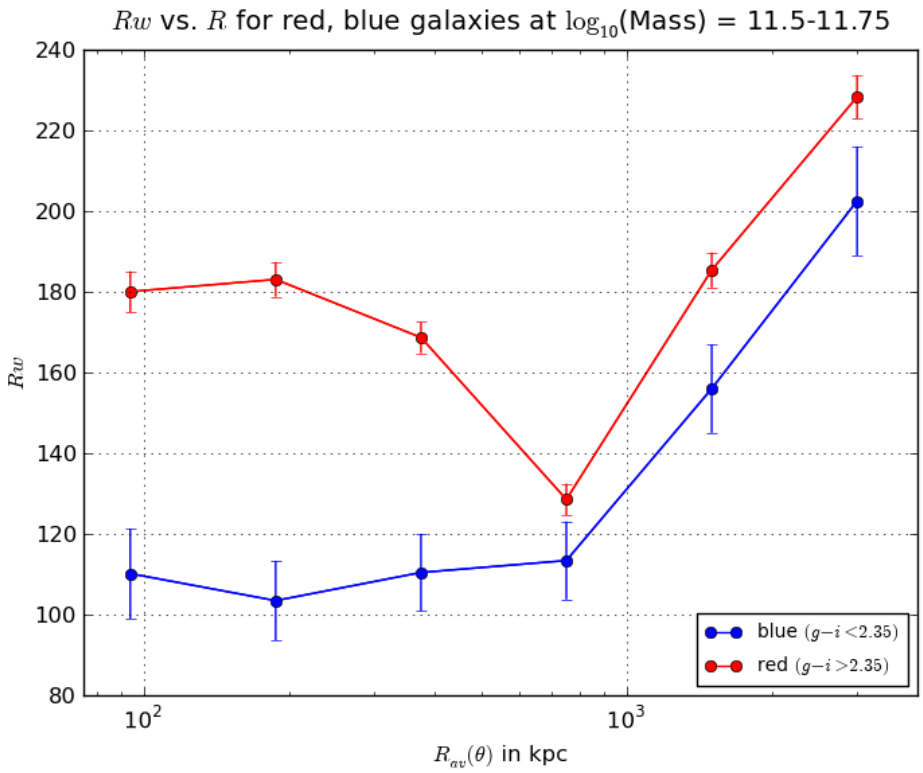

Fig. 13.— Rw vs. R for galaxies with $\log_{10}$(Mass) between 11.50 and 11.75. The differentiation between clustering in red and blue galaxies is even more pronounced here at smaller scales. Red galaxies show a dip as they approach radii of 1 Mpc.